Article Pre-Print

Dynamic Operability Analysis and Start-up of an Integrated Radiant Syngas Cooler and Steam Methane Reformer

Jaffer H. Ghouse, Dominik Seepersad, Thomas A. Adams II*

Department of Chemical Engineering, McMaster University, 1280 Main Street West, Hamilton, Ontario, L8S 4L7, Canada

**Corresponding author. Tel.: +1 (905) 525-9140 x24782; E-mail address: tadams@mcmaster.ca*

ABSTRACT

In our previous work, the modeling, design and steady-state performance of a novel integrated Radiant Syngas Cooler (RSC) of an entrained-bed gasifier and Steam Methane Reformer (SMR) was presented. The base-case designs that were established for both the co-current and counter-current configuration are used to evaluate the performance under a transient operating mode, evaluating the flexibility and feasibility to transition new operating steady-states. Each system, under open loop, is subjected to changes in key variables of the SMR feed on the tube side and disturbances to variables of the coal-derived syngas on the RSC side to determine the dynamics and stability of the integrated system. The results indicate that the co-current configuration is both more flexible and more inherently safe than the counter-current configuration, although it provides less cooling capability and has poorer methane conversion. In addition, the key variables that are more likely to violate the design limit in the event of a disturbance are identified thus aiding in the design of an effective control system. A realistic start-up procedure is also established for the integrated system based on current industrial practices that are employed for entrained-bed gasifiers and steam methane reformers.

***Keywords**: Steam Methane Reforming, Gasification, Integrated, Dynamic, Start-up, Polygeneration*

1. Introduction

In an entrained-bed gasifier, product synthesis gas (commonly called “syngas”, a mixture of hydrogen and carbon monoxide) exits the gasifier section at high temperatures of around 1350°C and has to be cooled for downstream unit operations [1]. The hot coal-derived syngas is cooled by employing a radiant cooler or quench cooling section or both in series. In the RSC section of conventional entrained-bed gasifiers, the cooling is provided by generating high pressure steam within tubes placed inside the radiant cooler. However, Adams and Barton [2] proposed a different cooling strategy by replacing high pressure steam generation with the highly endothermic steam methane reforming process. The proposed configuration while providing the required cooling to the hot coal-derived syngas also has other significant advantages:

(i) Increased system level efficiency as a result of process integration,

(ii) A valuable syngas stream with a high molar H_2/CO ratio (greater than 4) is produced via the steam methane reforming reactions.

(iii) In a number of industrial processes, coal-derived syngas, which has a low molar H_2/CO ratio, is upgraded using external reformers or water gas shift reactors to meet the feed requirements for downstream methanol synthesis and liquid fuels production. With the integrated configuration, the hydrogen rich syngas from methane reforming can be blended with the coal-derived syngas to meet the desired H_2/CO molar ratio.

Adams and Barton [2] showed that a polygeneration system which employed the integrated concept was technically feasible and economically desirable from a systems-level perspective. However, in their analysis, only a simple zero-order model was used for the integrated device which did not capture the complexities of high temperature heat transfer, heterogeneous reaction kinetics, and safety constraints on the temperature of the various materials used in its construction. As such, there were many unanswered questions about the range of operating conditions at which the device could safely operate,

how well it would perform, and what the actual design parameters should be (such as tube lengths, number of tubes, diameters, and arrangement).

To answer these questions, detailed dynamic heterogeneous models for the proposed integrated system were developed and analyzed [3]. The model accounted for spatial and temporal variations in key variables like temperature, concentration and pressure in the gas phase on the RSC shell and SMR tube side, where methane reforming reactions occur. The model was then utilized to develop a base-case design for two different configurations; co-current flow and counter-current flow. The results showed that a feasible design existed for both configurations subject to the process requirements and operating constraints but with different advantages and disadvantages for each configuration. For example, not only was the natural gas processing capacity higher for the counter-current configuration but a higher methane conversion of close to 90% was observed in the counter-current configuration. However, the disadvantage of the counter-current configuration was the proximity of the maximum tube wall temperature to the design limit of 1350 K. Furthermore, a sensitivity analysis was performed to assess the effect of certain model parameters on the overall performance. Finally, using the model for steady-state simulations, a base-case design for the proposed integrated configuration (co-current and counter-current) was established. The reader is referred to Ghouse et al. [3] for a complete description of the design heuristics, steady-state performance studies and the sensitivity results.

A flexible or “agile” polygeneration plant in which the feeds and/or products are changed seasonally, weekly, or even daily in response to market conditions could yield significant financial benefits. For example, Chen et al. [4] demonstrated that if each subsection of a polygeneration process had enough flexibility to transition between 50% and 100% of its maximum capacity on a daily basis, the net present value of the plant could respond to market conditions over the course of its life time enough to increase its net present value by 17% compared to a plant that always operates at the same steady-state. At maximum flexibility (between 0% and 100% of capacity), the net present value increases up to 62%.

Similarly, one of the main advantages of the proposed device is that it can be used in a similar fashion, changing the feed amounts or product amounts in response to market conditions. However, with the proposed design, the gasifier itself remains at steady state, which is a desirable property since gasifiers are rarely used dynamically in an industrial setting at least with the current generation of gasifiers.

Therefore the main objective of this work is to study the flexibility of the integrated device in the context of a polygeneration plant. The quality of the syngas produced from the integrated system can be altered by manipulating the operating variables. However, it is critical to ensure that such transitions to new operating points are safe and feasible. This study helps in determining the safe operating envelope and the extent to which it can be used for agile polygeneration. Furthermore, the effect of gasifier disturbances on the system performance and a start-up procedure is established and simulated.

2. Flexibility in syngas yield and H_2/CO ratio for downstream processes

As mentioned in the introduction, one of the key advantages anticipated for the proposed integrated system is the ability to vary the molar H_2/CO ratio of the blended syngas (hydrogen and carbon monoxide) depending upon the downstream process requirements, thereby eliminating the need for upgrading the coal-derived syngas using water gas shift reactors. For the designs that were established previously, the production rates and mole fraction of the syngas produced at steady-state is listed in Table 1 [3]. The coal-derived syngas and reformed syngas can be blended in different ratios to get the desired H_2/CO molar ratio in the blended syngas. However, the amount of blended syngas available at a particular H_2/CO ratio limits the final yield of the desired products. To this end, two different blending modes are used for this study for a polygeneration plant; Mode 1 and 2. Mode 1 uses all of the available coal-derived syngas and different fractions of the reformed syngas for blending while Mode 2 uses all of the reformed syngas and different fractions of the coal-derived syngas are added to the blend. Figure 1

and 2 shows the production capacity of the blended syngas for different molar H_2/CO ratios for co-current and counter-current configurations respectively.

Table 1:

Parameter	Co-current Design		Counter-current Design	
	Reformer	Gasifier	Reformer	Gasifier
Natural Gas/Coal Feed (TPH)	17	102	19	102
Syngas Produced (TPH)	20	123	27	123
Product Composition:				
Methane	0.032	-	0.018	-
Water	0.355	0.166	0.343	0.137
Carbon Monoxide	0.075	0.332	0.096	0.304
Hydrogen	0.452	0.359	0.469	0.387
Carbon Dioxide	0.061	0.143	0.049	0.172

Figure 1 shows that for the co-current configuration, the molar H_2/CO ratio ranges from 1.1 (pure coal-derived syngas) to 6 (pure reformed syngas). Using mode 1, the H_2/CO ratio can be varied from 1.1 to 1.6 with a corresponding minimum capacity of 123 TPH to a maximum capacity of 143 TPH when 100% of the reformed syngas is used for blending with the coal-derived syngas. The resulting H_2/CO ratio from mode 1 is compatible for Dimethyl Ether (DME) synthesis for which the feed molar H_2/CO ratio requirement typically ranges from 1.2-1.5 [5]. On the contrary, mode 2 yields a molar H_2/CO ratio between 1.6 and 6. In mode 2, the molar H_2/CO ratio of 2 that is desirable for Fischer-Tropsch (FT) liquids [6] or methanol production [7] is achieved by blending 50% of the coal-derived syngas with the reforming derived syngas. Furthermore, higher molar H_2/CO ratios are available for hydrogen production although at lower syngas flow rate of 20 TPH. For the counter-current configuration, shown

in figure 2, the operating line for syngas flow rates versus the molar H_2/CO ratio is similar to that of the co-current configuration. However, the quality of the blended syngas is different for counter-current configuration. For example, the H_2/CO ratio of pure coal-derived syngas is higher at 1.3 owing to the increased water gas shift reaction in the radiant cooler for the counter-current design. The yield of syngas suitable for DME synthesis is lower than that available for the co-current design but the requirement is achieved by blending just 35% of the reformed syngas with the coal-derived syngas. Also, at maximum yield of 141 TPH, the syngas H_2/CO ratio is higher at 1.85. For FT synthesis, the amount of syngas is available is 101 TPH which is 25% higher than the amount available for the co-current design. The disadvantage with the design may be the maximum H_2/CO ratio that can be achieved with the counter-current configuration is 4.8 that may limit the production of high purity hydrogen. This shows that there are different advantages to be gained with the co-current and counter-current configurations. It is also important to note that the aforementioned flexibility analysis in syngas H_2/CO ratios and capacity for polygeneration is done at steady-state. In the following sections, the ability to safely alter the operating envelopes shown in Figure 1 and 2 will be analysed.

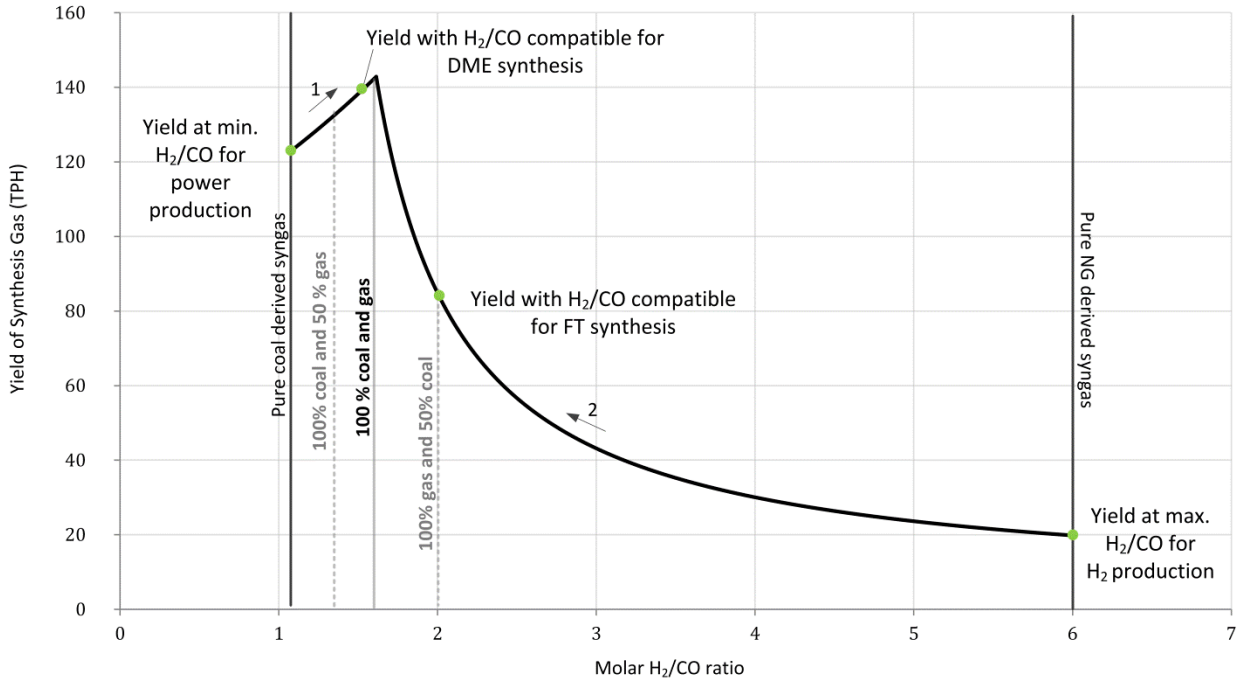

Figure 1: Syngas yields with different molar H_2/CO ratios for the co-current configuration

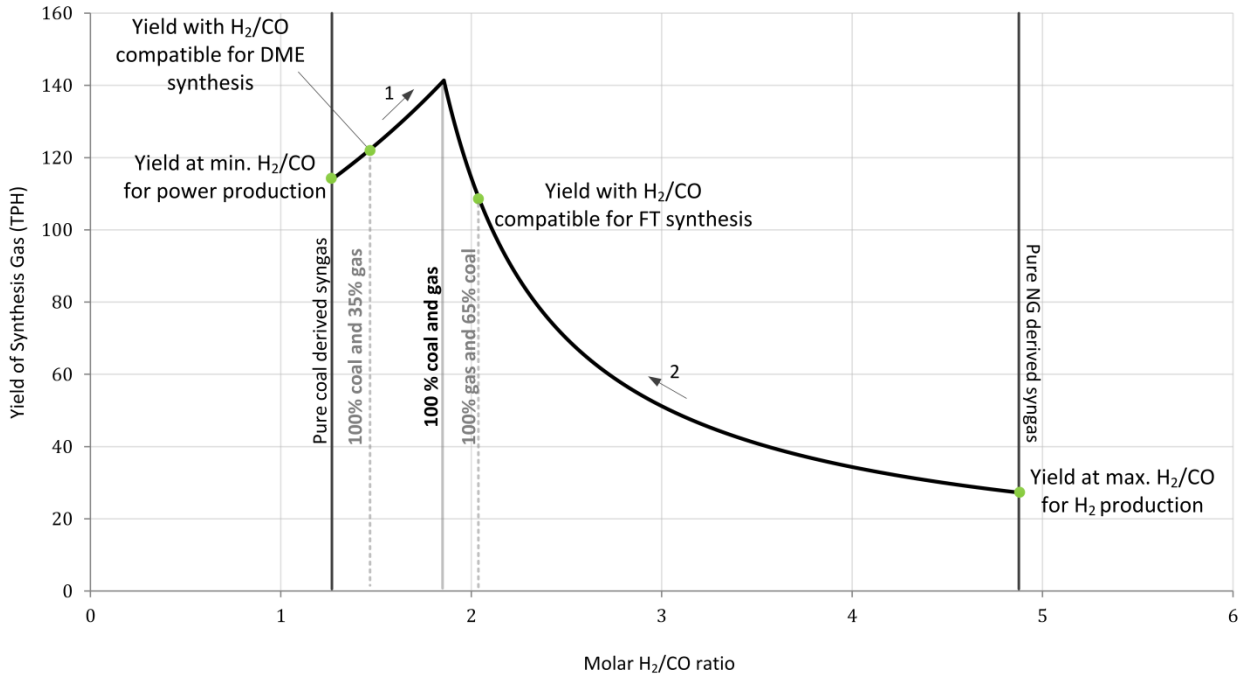

Figure 2: Syngas yields with different molar H_2/CO ratios for the counter-current configuration

3. From Steady-state to Dynamic simulations

The model for the integrated system was implemented and solved in gPROMS v3.7.1 [8]. The system of partial differential and algebraic equations were discretized in space using the method of finite differences. The reader is advised to refer to Ghouse et al. [3] for a detailed account on the solution techniques and grid size employed to simulate the integrated system. The steady-state operating point that was established for the co-current and counter-current configuration (outlined in Table 1) was used as the initial state for all the dynamic simulations presented in this work to mimic a scenario where the system is subjected to changes from a steady-state operating point. To achieve this in gPROMS, the following commands are used: (i) “SAVE”, (ii) “RESTORE” and (iii) “REASSIGN”. The “SAVE” function saves the state of all variables at any point (the steady-state operating point in this instance) while the “RESTORE” function is used to restore a saved variable set to initialize the simulation from that particular operating point, and the “REASSIGN” function is used to change input variables to the model (i.e. inducing step changes or disturbances to the system).

In this work, dynamic case studies are performed in open loop to assess the system dynamics and determine constraints that might impede the desired dynamic operability characteristics of the integrated system. Furthermore the integrated system is subjected to disturbances on the shell to determine unsafe operating conditions, if any. It should be noted that unlike traditional steam methane reformers where the heat supply to the tubes can be altered effectively by controlled firing of the burners in the furnace [9], the heat supply to the reformer tubes cannot be controlled in the case of the proposed integrated system as the heat is from the coal-derived syngas on the shell side. This leads to a difficult but interesting scenario in which the integrated system can only be controlled with the SMR tube side variables while treating any change on the shell side as a disturbance and simultaneously ensuring that the required cooling duty is provided to the coal-derived syngas and the operating constraints are not violated.

3. Tube Side Variables

3.1 Effect of feed inlet temperature (+/- 50 K)

The feed temperature on the tube side was subjected to a step change of +/-50 K at time 500s. Figure 3 shows the effect of the step change on exit tube and shell gas temperatures, catalyst core temperature at different axial positions along the length of the reactor, change in steady-state outer tube wall temperatures and methane conversion for the co-current configuration. Figure 3A shows that the exit tube gas temperature shows inverse response and changes by 4 K for a +/- 50 K change in feed temperature while the shell gas temperature changes by 6 K. Though there is a 75s lag before changes are noticeable at the shell exit, the dynamics of the system fast approaches a new steady-state after 450s. Also, from Figure 3C it is observed that the change in catalyst core temperatures at different axial positions is negligible except at the inlet where the temperature change reflects the change in the inlet gas temperature. The new steady-state temperature for the outer tube wall does not violate the design limit and the change from the previous steady-state is uniform throughout the length except between 0.5 m and 3 m as shown in Figure 3B. The reason for this change in trend is that a +50 K step change in temperature at the inlet speeds the endothermic reaction thus reducing the temperature while a -50 K step change slows the endothermic reaction thus increasing the temperature. However the same effect is not reflected along the remaining length of the tube. For the most part, the step changes in feed inlet temperature do not affect the methane conversion significantly with the resulting change being only around 2.5 percentage points as shown in Figure 3D. The inlet gas temperature has an inverse response on the syngas H_2/CO ratio. For +/- 50 K change in the feed temperature, the molar H_2/CO ratio of the syngas changes from 6 to 5.8 and 6.2 respectively. The magnitude of change in the H_2/CO ratio can be greater if the change in the inlet gas temperature is larger.

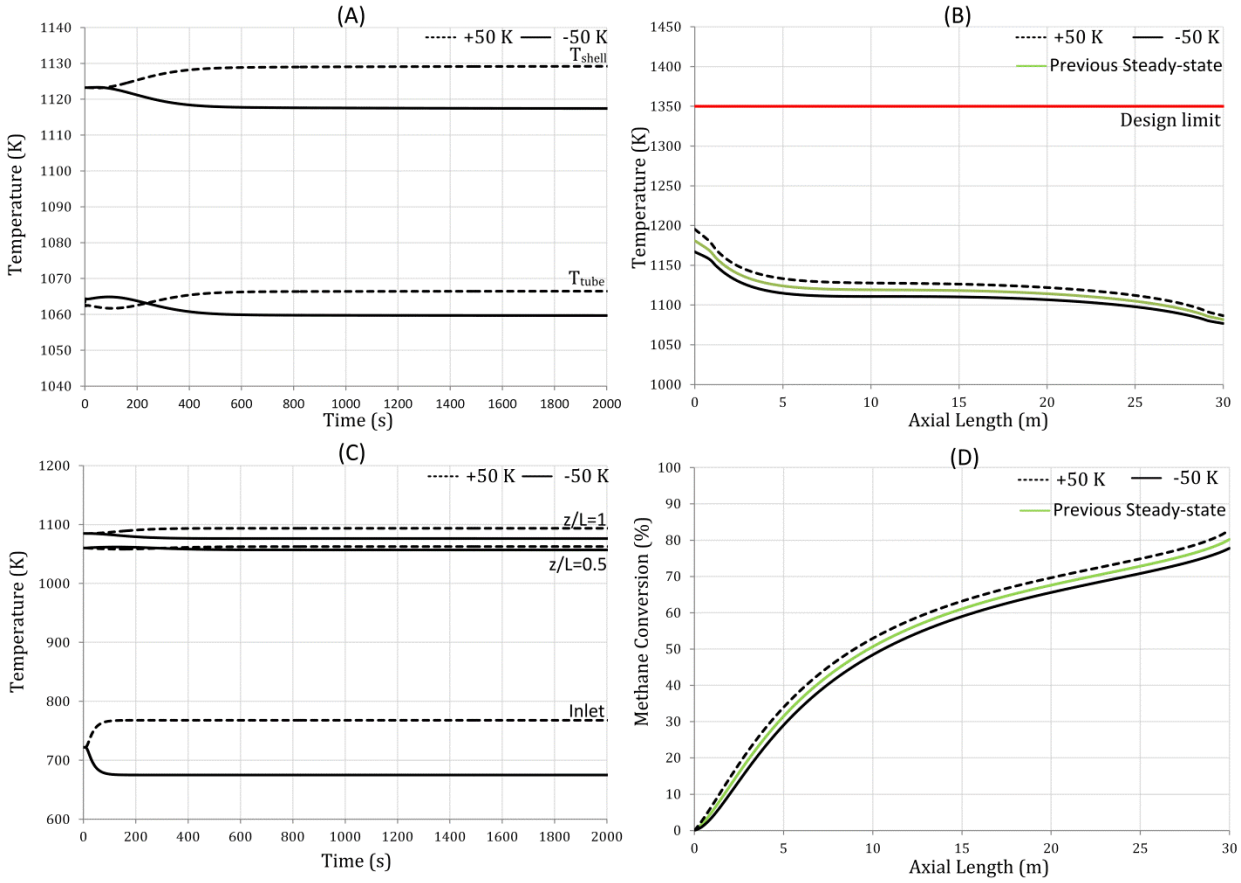

Figure 3: Effect of step change of both +50 K and -50 K in inlet temperature for co-current configuration on (a) exit gas temperature leaving the tube and shell, (b) axial tube wall temperature, (c) catalyst core temperature at the inlet, exit, and halfway point and (d) axial methane conversion.

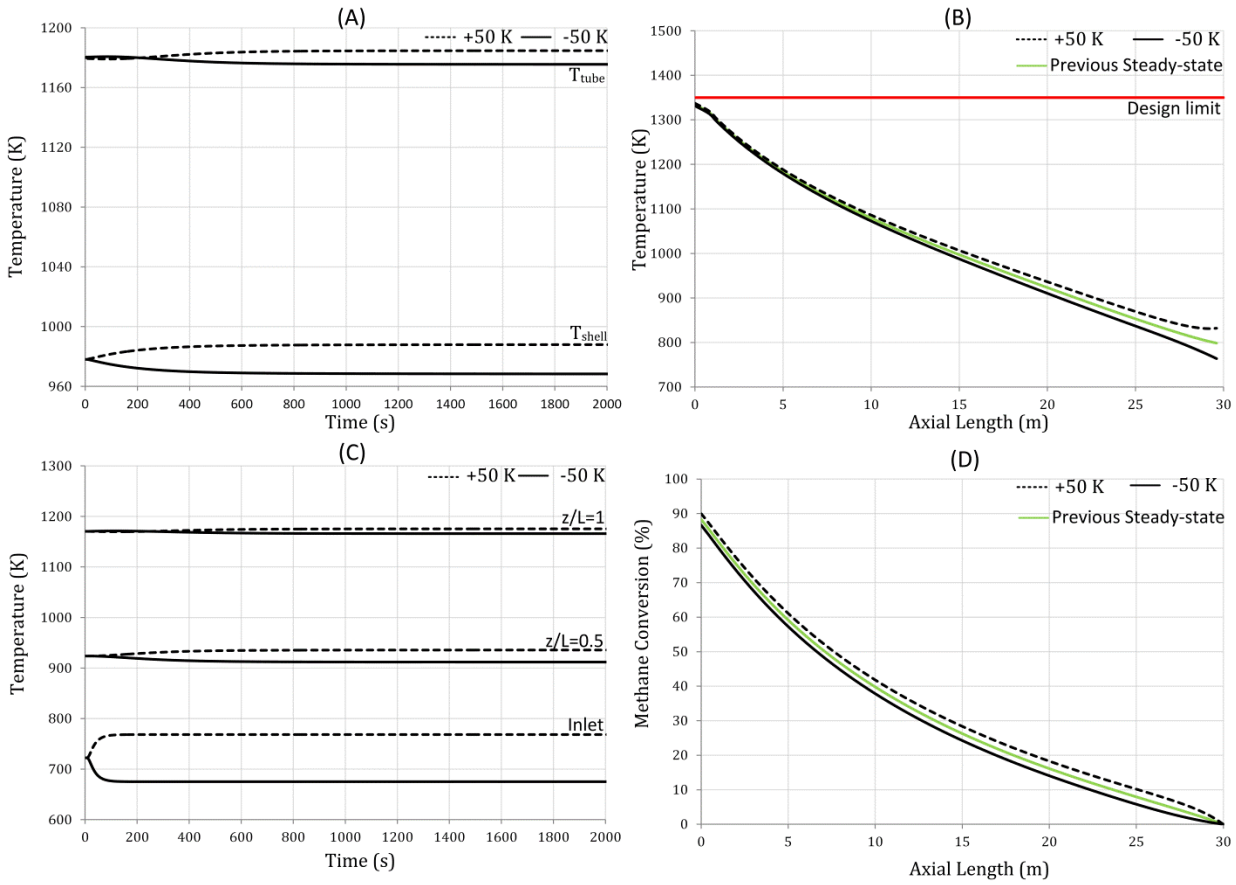

Figure 4: Effect of step change of both +50 K and -50 K in inlet temperature for counter-current configuration on (a) exit gas temperature leaving the tube and shell, (b) axial tube wall temperature, (c) catalyst core temperature at the inlet, exit, and halfway point and (d) axial methane conversion.

For the counter-current configuration the effect of a similar step change in the inlet feed temperature is shown in Figure 4. Figure 4A shows that the exit shell gas temperature changes by around 5 K while the exit tube gas phase temperature changes by around 10 K. Though the change in exit gas phase temperature appears to be similar to the co-current configuration, an interesting difference is the time required for the impact of the step change to be reflected at the shell and tube exit for each configuration. The change is reflected immediately in the gas temperature on the shell side because of its proximity to the source of the inlet step change owing to the counter-current configuration, while for the tube exit the time required to reflect the change is around 200s; slower than that for the co-current configuration. With the exit gas temperature usually being the measured variable in conventional SMR

systems, the change in the dead time between co-current and counter-current configurations will affect the control design and its efficacy. For the catalyst core temperatures, the change is minor, around 10 K, except at the inlet where the step change occurs. However, the magnitude of the change in the steady-state outer tube wall temperature along the axial length varies and is not a constant as seen in the co-current configuration. This change ranges from 33 K at z=30 m (inlet for the tube side) to around 4 K at z=0 m (exit for the tube side). Therefore a +50 K change in feed temperature results in the maximum tube wall temperature approaching the design limit temperature. Also, a similar drop in tube wall temperature close to the inlet is observed owing to the speed of the endothermic reaction. However, the change in methane conversion is 1.7 percentage points which is lower when compared to the co-current configuration. For the counter-current design, the molar H_2/CO ratio changes to 5 when the inlet temperature is reduced by 50 K and to 4.8 when the inlet temperature is increased by 50 K.

3.2 Operating at a lower steam to carbon ratio

Steam is one of the reactants for both the SMR reaction and the water gas shift reaction that occurs in parallel within the tubes. Furthermore, the change in feed steam supply affects the H_2O/C ratio which affects the rate of total methane conversion. In conventional SMR reactors, the typical H_2O/C ratio is greater than 3. One of the other reasons to maintain a high ratio, apart from promoting higher conversion, is to avoid carbon deposition that occurs at H_2O/C ratios of less than 1 [10]. Steam supply is also crucial for driving the forward endothermic reactions thereby consuming the high heat supplied to the SMR tubes; failure will lead to overheating of the catalyst and tube walls. Furthermore, the inlet H_2O/C ratio has a significant impact on the molar H_2/CO ratio in the reformed syngas. Therefore, in the following section a 50% reduction in steam supply is simulated which results in an inlet H_2O/C ratio of 1.6.

For the co-current configuration, the steam supply was reduced by 50% and introduced as a step change. The effect of the change in the inlet H_2O/C ratio on the exit tube and shell gas temperature, tube wall temperature, catalyst core temperature and methane conversion is shown in Figure 5. Figure 5A shows that the exit gas temperature on both the shell and tube side increase owing to the net reduction in flow rate on the tube side. The tube gas exit temperature increases by 118 K while the change in shell gas exit temperature is lower at 72 K. Though the temperature of the gas phase increases, the rate of the endothermic reaction decreases as a result of decreased reactant concentration and this is reflected in the decrease in methane conversion by 18 percentage points from the base-case 80% as shown in Figure 5D. Figure 5C shows that the catalyst core temperature increases slowly but the change in temperature is around 76 K at 15 m and 120 K at the exit. The outer tube wall temperatures also show a significant change. The temperature increases near the inlet by 43 K but at the centre and exit the temperature increases by around 71 K and 104 K respectively. However, the maximum tube wall temperature is well within the specified design limit temperature of 1350 K. Though the system is able to handle the step change without violating any set constraints, it is hard to determine if the commercial catalyst and tube walls can handle the rate of temperature increase in a short time. However, it should be noted that here the change was introduced as a step change and such sharp increase in temperatures can be avoided by subjecting the system to a ramp change or a series of small step changes. Furthermore, the effect of a low H_2O/C ratio has a significant effect on the product molar H_2/CO ratio. The molar H_2/CO ratio decreases from 6 to 4 when the inlet H_2O/C ratio is reduced from 3.3 to 1.6. Therefore, the inlet steam can be used to manipulate the reforming syngas molar H_2/CO ratio as desired for downstream process requirements. These results also show that the H_2O/C ratio can be potentially used as a manipulated variable to control the rate of reaction without violating any of the set constraints.

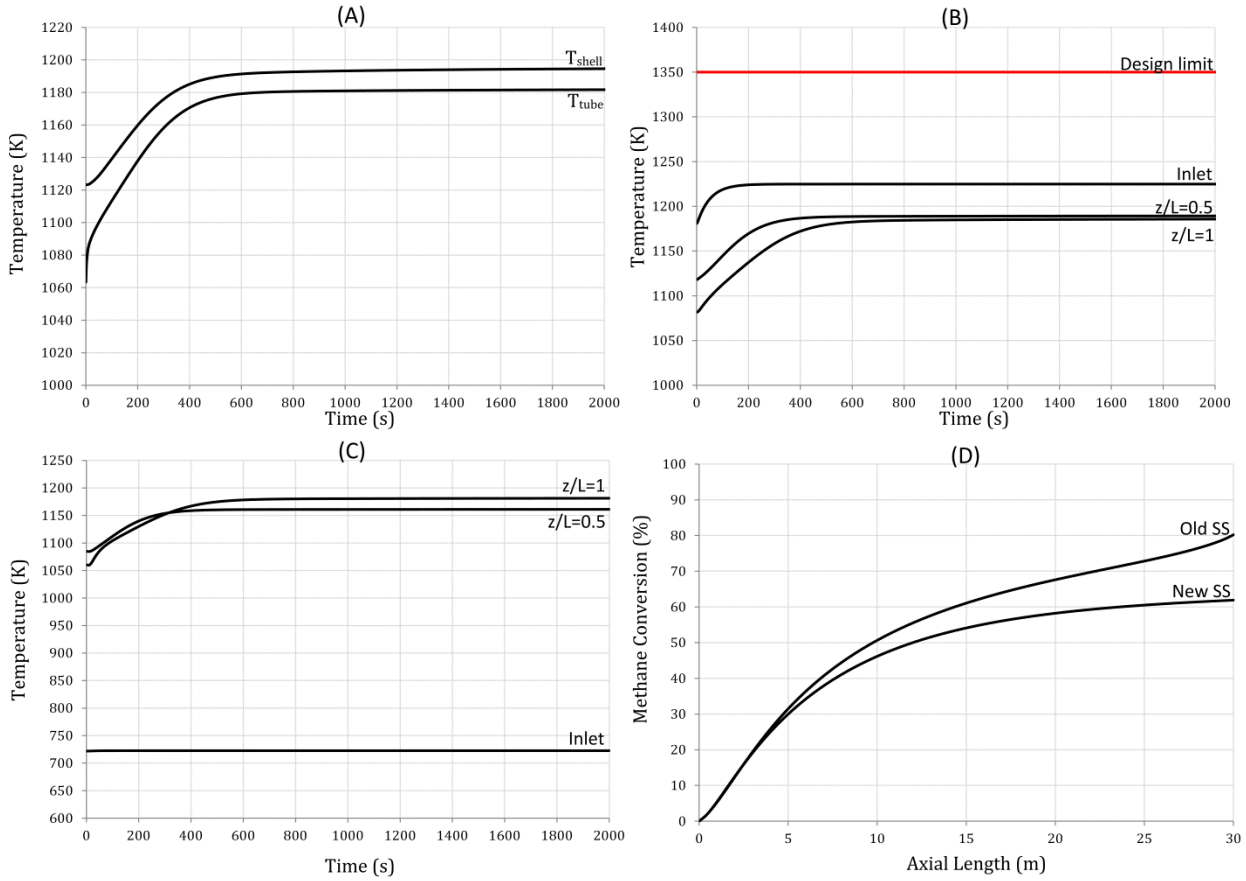

Figure 5: Effect of 50% reduction in inlet steam supply for co-current configuration on (a) exit gas temperature leaving the tube and shell, (b) tube wall temperature at the inlet, exit, and halfway point, (c) catalyst core temperature at the inlet, exit, and halfway point and (d) axial methane conversion.

A similar change was simulated for the counter-current configuration and its effect on shell and tube exit gas temperature, outer tube wall temperature, catalyst core temperature and methane conversion is shown in Figure 6. In Figure 6A, it can be seen that the tube exit gas temperature changes by as much as 126 K while the shell gas exit temperature changes by 45 K. As observed in the co-current configuration, the catalyst core temperature changes significantly; 129 K at the tube gas exit and 88 K at 15 m. Though the methane conversion drops by only 10 percentage points shown in Figure 6D, the major drawback is that the outer tube wall temperature near the tube gas exit breaches the design limit in 15s as shown in Figure 6B. It is important to note that the base case steady-state maximum tube wall

temperature was very close to 1350 K which limits its flexibility for transient modes of operation. For the counter-current configuration, the product molar H_2/CO ratio decreases from 5 to 3.5 but is irrelevant as the design cannot safely transition to a new operating steady-state.

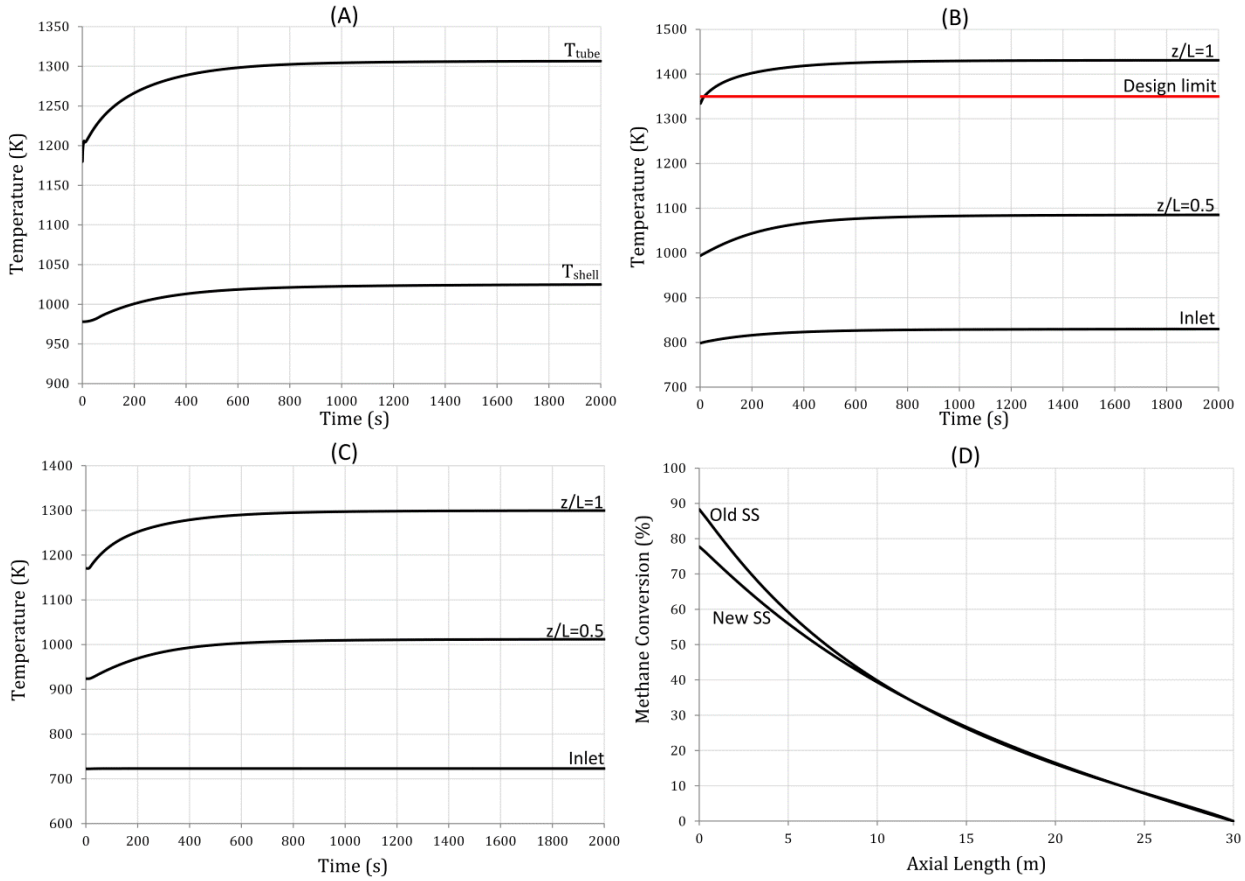

Figure 6: Effect of 50% reduction in inlet steam supply for counter-current configuration on (a) exit gas temperature leaving the tube and shell, (b) tube wall temperature at the inlet, exit, and halfway point, (c) catalyst core temperature at the inlet, exit, and halfway point and (d) axial methane conversion.

3.3 Operating the reformer at reduced capacity

As mentioned previously in section 1, one of the advantages that were envisaged for the proposed integrated system was the flexibility to operate it dynamically. The feed flow to the SMR tubes (containing the mixture of steam and natural gas) is subjected to a step decrease of 25% to simulate a scenario where the demand for products is low and to determine if the integrated system can handle a

lower throughput. The effect on gas exit temperatures, outer tube wall temperatures, catalyst core temperatures and methane conversion for the co-current configuration is shown in Figure 7. Figure 7A shows that the exit gas phase temperatures on both the shell and tube sides increase owing to lower throughput through the tubes and reach a new steady-state in 600 s. The magnitude of change of the shell gas temperature is 65 K while for the tube gas temperature it is 110 K. Though the shell gas exit temperature increases to 1188 K, the increase in temperature can be easily handled by the downstream quench cooler [11]. Also, from Figure 7B it can be observed that though the outer tube wall temperature increases, it is still well within the design limit. The rate of temperature increase is faster at the inlet than at other positions along the axial length. Figure 7C shows that the catalyst core temperature at the centre and at the exit changes by 67 K and 113 K respectively. Owing to the increase in temperature of the gas and catalyst phase, the endothermic reactions move forward resulting in a higher methane conversion of 83% from the previous 80% as shown in Figure 7D. Figure 8 shows the effect of the reduced reformer feed on the yield of blended syngas and molar H_2/CO ratio. The operating envelope shifts to the left of the steady-state operating point where the maximum yield of syngas remains nearly constant but with different H_2/CO ratios. The turn down in reformer feed may be beneficial for downstream processes. For example, the available syngas feed drops by almost 40% for FT synthesis and 20% for DME synthesis which may be beneficial when the production of liquid fuels has to be decreased as the plant moves towards more power production during the day time. The results further demonstrate the effect of the system temperature on the H_2/CO ratio of the syngas – an increase in temperature affects the rate of the WGS reaction that decreases the moles of hydrogen and increases the moles of carbon monoxide in the syngas.

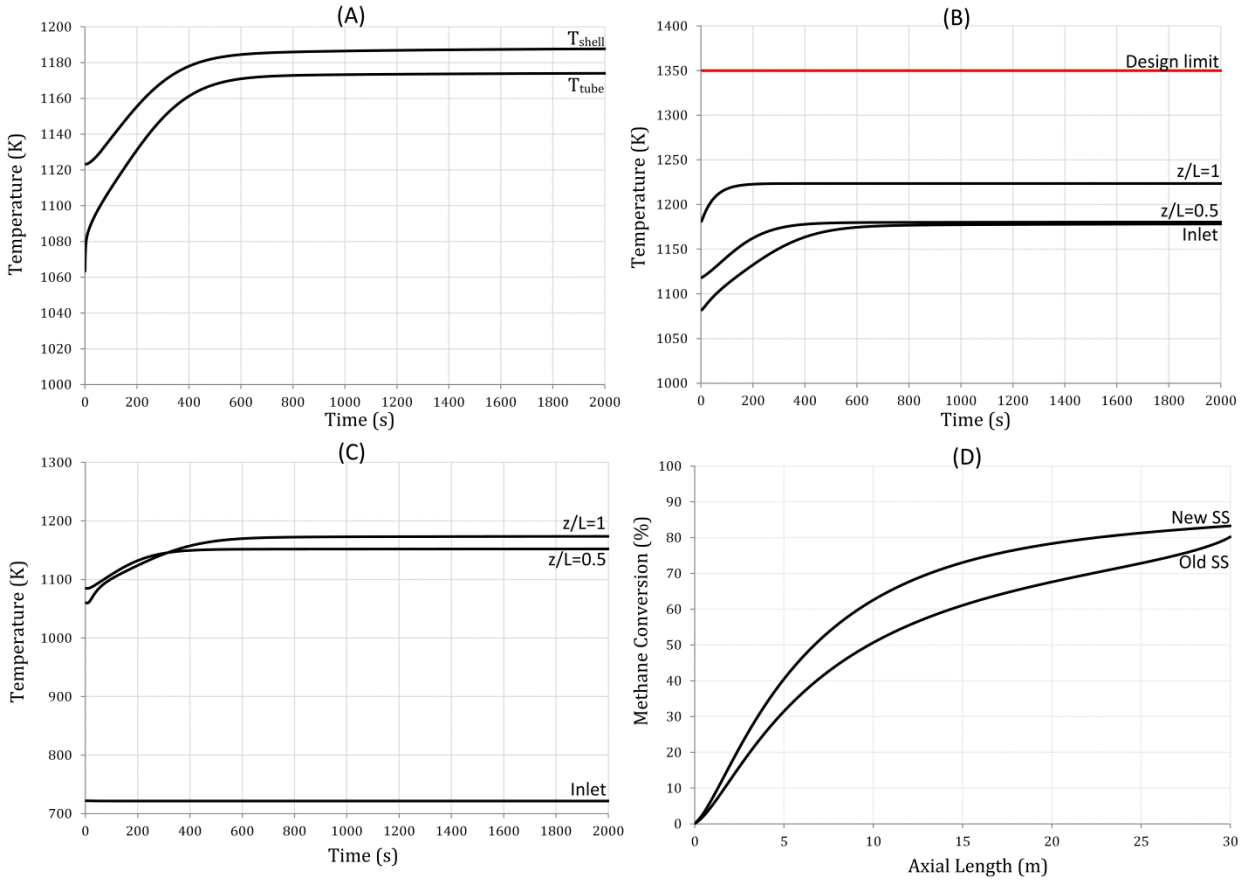

Figure 7: Effect of step decrease in total SMR feed by 25% for co-current configuration on (a) exit gas temperature leaving the tube and shell, (b) tube wall temperature at the inlet, exit, and halfway point, (c) catalyst core temperature at the inlet, exit, and halfway point and (d) axial methane conversion.

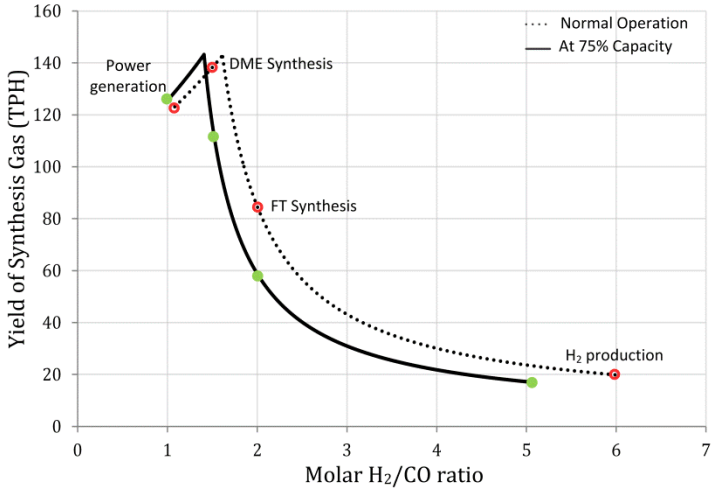

Figure 8

For the counter-current configuration, the effect of a step decrease in feed flow to the SMR tubes is shown in Figure 9. Figure 9A shows that the change in shell gas exit temperature is only 20 K while the tube gas exit temperature increases rapidly to 1350 K. As observed with other case studies for counter-current configuration, Figure 9B shows that the outer tube wall temperature exceeds the design limit immediately at the tube exit. The catalyst core temperature near the exit increases by 180 K which can damage the catalyst; although such hot spots are not observed at any other axial position as shown in Figure 9C. Owing to the very high temperature, the methane conversion reaches as high as 96%, though this is irrelevant since the step change leads to tube material failure. This result clearly demonstrates that the counter-current configuration is not as flexible as the co-current configuration to handle lower feed rates. This means that the co-current configuration may be more desirable from a systems perspective, since the increased flexibility would enable more flexibility of the polygeneration system in which it is used.

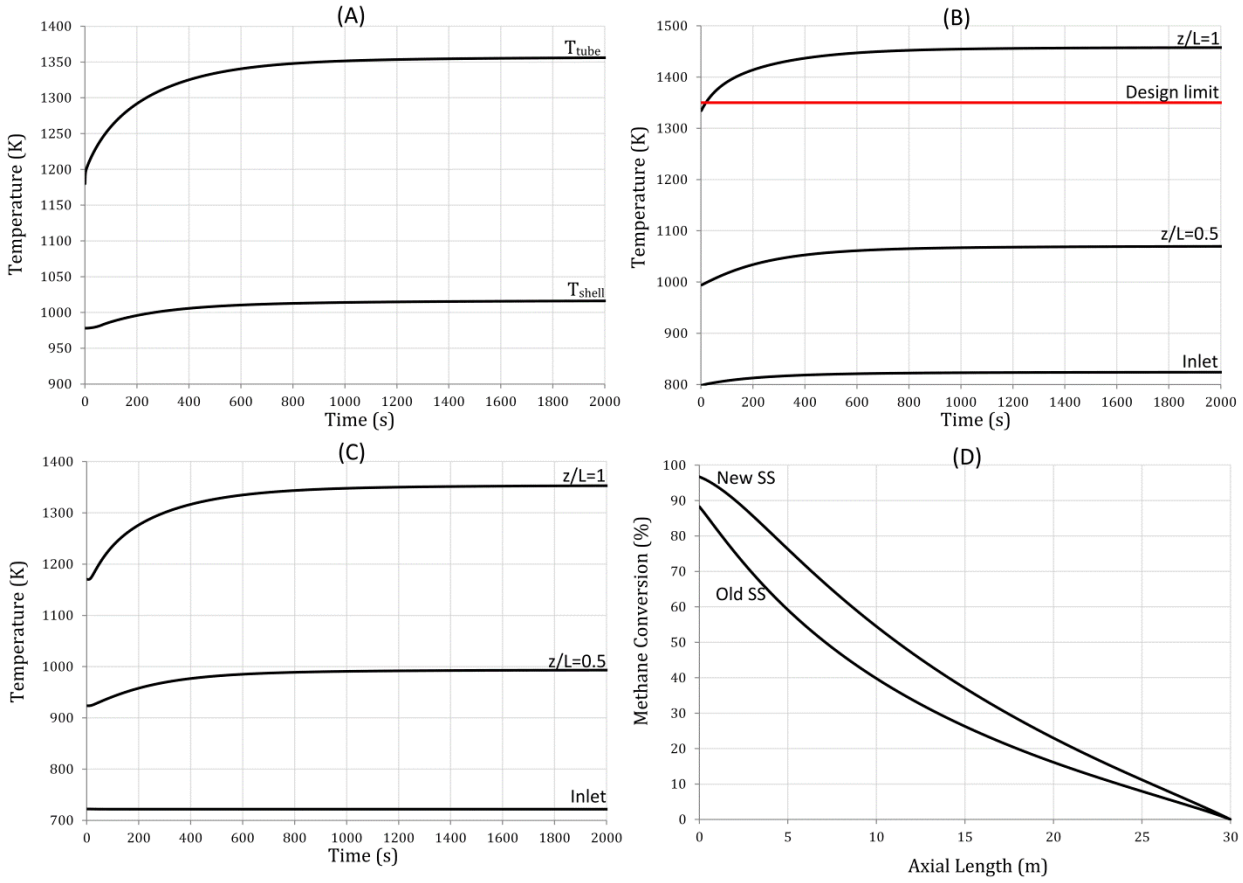

Figure 9: Effect of step decrease in total SMR feed by 25% for counter-current configuration on (a) exit gas temperature leaving the tube and shell, (b) tube wall temperature at the inlet, exit, and halfway point, (c) catalyst core temperature at the inlet, exit, and halfway point and (d) axial methane conversion.

4. Shell Side Variables

In this section, changes are made to the shell side variables at the inlet of the RSC. As these variables cannot be controlled in the integrated system, the changes are considered to be disturbances rather than step changes in controlled inputs. However, one case study is presented where the flow rates on the shell side are decreased by 50% to simulate load following scenarios of advanced gasifiers that can operate dynamically.

4.1 Fluctuations in inlet temperature

The inlet shell gas temperature was subjected to a +25 K disturbance for 300s. The response of different variables on the shell and tube side is shown in Figure 10. Figure 10A shows the tube gas phase temperature at different lengths along the axial domain. It can be seen that the change in gas phase temperature is only around 8 K along the entire length. Also, for the response to be reflected at the tube exit takes considerable time owing to the co-current configuration. The results show that the integrated system is capable of handling the temperature disturbance as the exit shell gas temperature increases by only about 6 K before returning to the previous steady-state point shown in Figure 10B. Figures 10C and 10D show that the tube wall temperature and catalyst core temperature are not affected by much. The outer tube wall temperature at the inlet shows a maximum change of 19 K before returning to the nominal operating temperature. Furthermore, the mole fraction profiles on both the shell and tube exit do not show any change and the system is able to survive the temperature disturbance easily even when operating in open loop. Though a larger disturbance than 25 K could have been simulated, it is rare that significant changes to the gasifier exit temperatures occur during operation even at reduced loads [12].

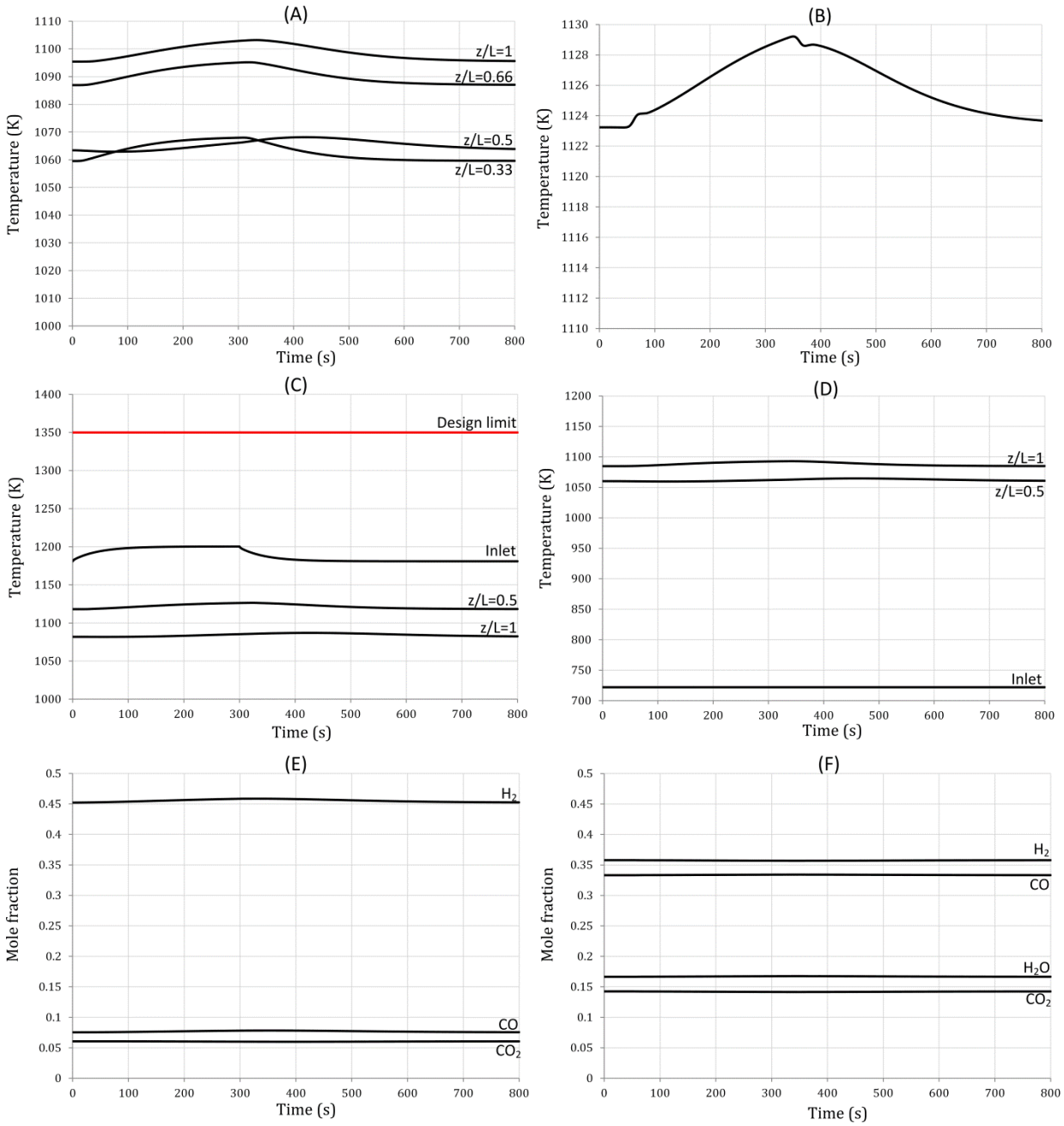

Figure 10: Effect of +25 K disturbance in inlet shell temperature for 300s in co-current configuration on (a) tube gas temperature at different axial points, (b) exit shell gas temperature, (c) tube wall temperature at the inlet, exit, and halfway point, (d) catalyst core temperature at the inlet, exit, and halfway point, (e) exit tube syngas mole fraction and (f) exit shell syngas mole fraction.

A similar disturbance was introduced for the counter-current configuration and the response is shown in Figure 11. Figure 11A shows the effect of the disturbance on the tube gas phase temperature at different positions along the axial length. Unlike the co-current configuration, where the effect is observed across the entire length, the effect is seen only at the tube exit because of the mode of operation with the tube exit being close to the point of disturbance. In addition, the shell exit temperature changes by a maximum of 2 K showing that the system is able to handle the disturbance effectively. Figure 11C shows that the outer tube wall temperature near the tube exit exceeds the design limit by a maximum of 20 K for a period of 220s during which the disturbance occurs. Though the catalyst core temperature and exit mole fraction profiles on the shell and tube side stay approximately constant, the ability of the counter-current configuration to handle the disturbance depends on the tube material that will be used.

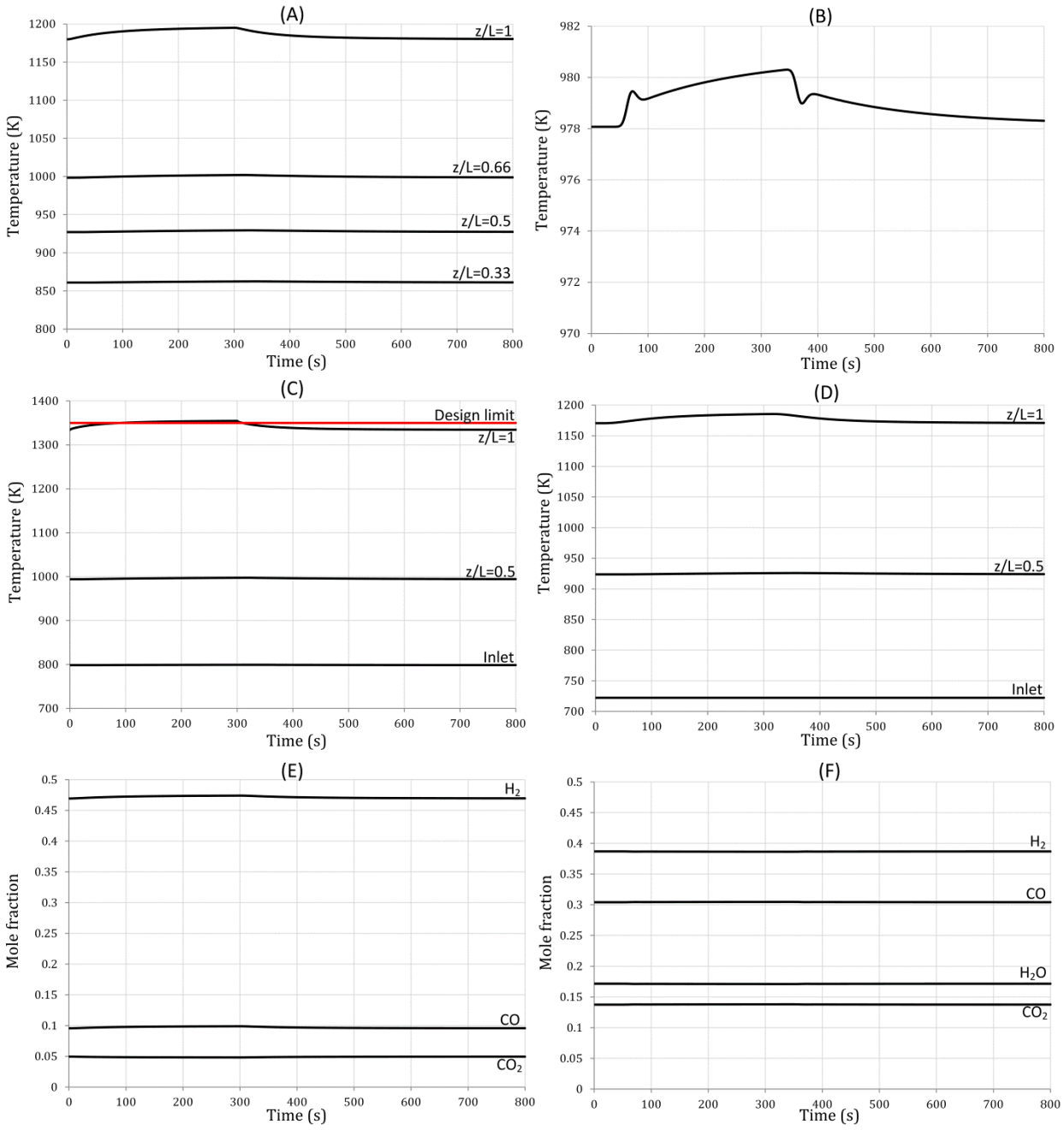

Figure 11: Effect of +25 K disturbance in inlet shell temperature for 300s in counter-current configuration on (a) tube gas temperature at different axial points, (b) exit shell gas temperature, (c) tube wall temperature at the inlet, exit, and halfway point, (d) catalyst core temperature at the inlet, exit, and halfway point, (e) exit tube syngas mole fraction and (f) exit shell syngas mole fraction.

4.2 Inlet flow rate disturbance

A shell-side inlet flow rate disturbance of 5% was simulated for both the co-current and counter-current configurations for 300s and the response of the key variables is shown in Figures 12 and 13 respectively. The exit shell and tube gas temperatures, shown in Figure 12A for the co-current configuration, change marginally by a maximum of 8 and 5 K, while the outer tube wall temperature and catalyst core temperatures along the axial length show negligible change from their steady-state values. The disturbance has a minor effect on the SMR reactions inside the tubes as shown by the exit mole fraction profiles in Figure 12D. The counter-current configuration also responds in a similar way and is able to survive the disturbance in open loop with no loss in performance.

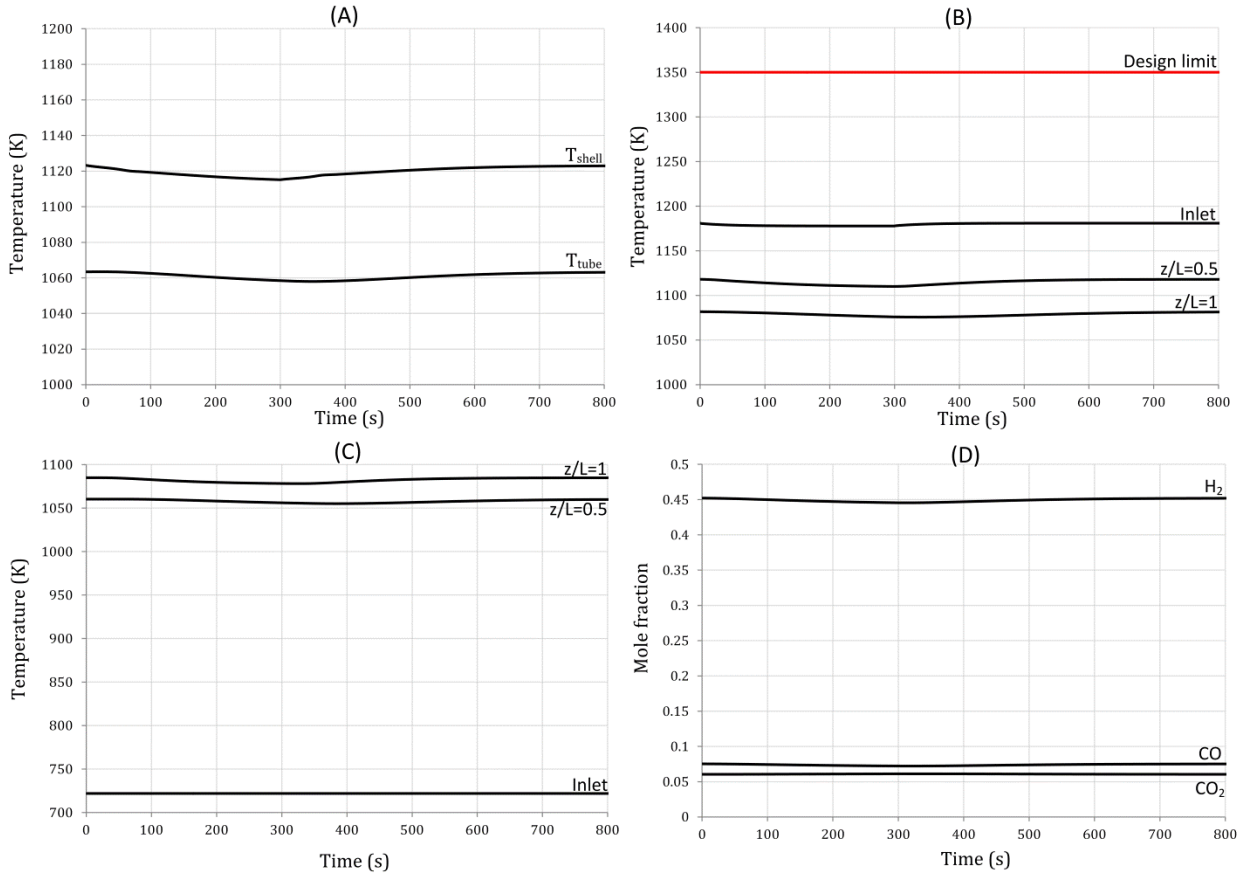

Figure 12: Effect of 5% disturbance in inlet shell flow rate for 300s in co-current configuration on (a) exit gas temperature leaving the tube and shell, (b) tube wall temperature at the inlet, exit, and halfway point, (c) catalyst core temperature at the inlet, exit, and halfway point and (d) tube side exit syngas mole fraction.

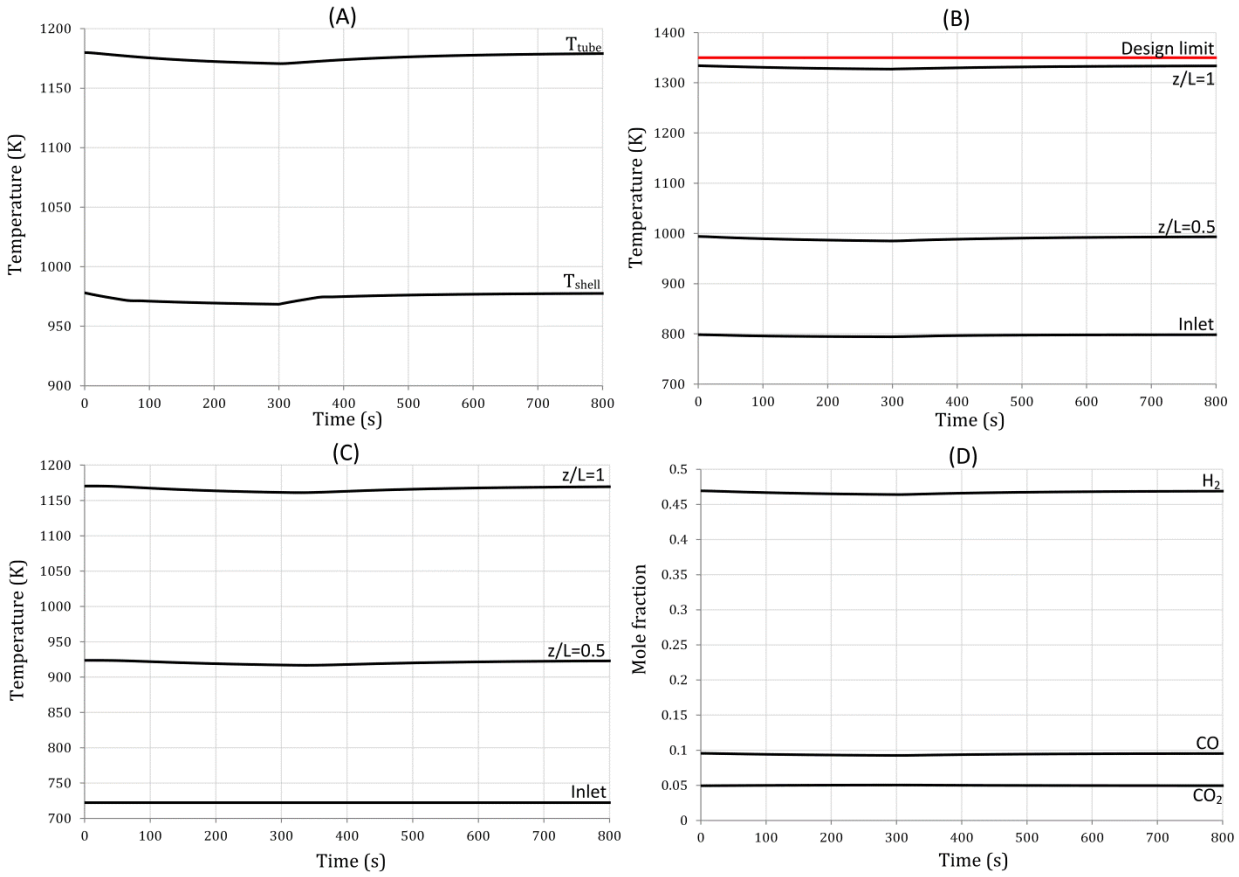

Figure 13: Effect of 5% disturbance in inlet shell flow rate for 300s in counter-current configuration on (a) exit gas temperature leaving the tube and shell, (b) tube wall temperature at the inlet, exit, and halfway point, (c) catalyst core temperature at the inlet, exit, and halfway point and (d) tube side exit syngas mole fraction.

4.3 Step decrease in feed flow (50% drop)

A step decrease of 50% in the coal-derived syngas at the RSC inlet was simulated. For the co-current configuration, the resulting effect on key variables is shown in Figure 14. Figure 14A shows that the exit gas phase temperatures on both shell and tube sides decrease slowly and take 1000s to reach new steady-states. The coal-derived syngas is further cooled to around 1000 K owing to higher residence time in the RSC and no change in flow rates on the tube side. Following a similar trend, the tube wall

temperature and catalyst core temperature also decrease as shown in Figure 14B and 14C. With the heat supply to the tubes decreasing owing to reduced throughput on the shell side, the methane conversion drops significantly to 50%. However the response here is in open-loop, and it will be interesting to see if an efficient control system can manintain the desired exit methane conversion and product mole fraction by regulating the inlet feed flow rate to the tubes.

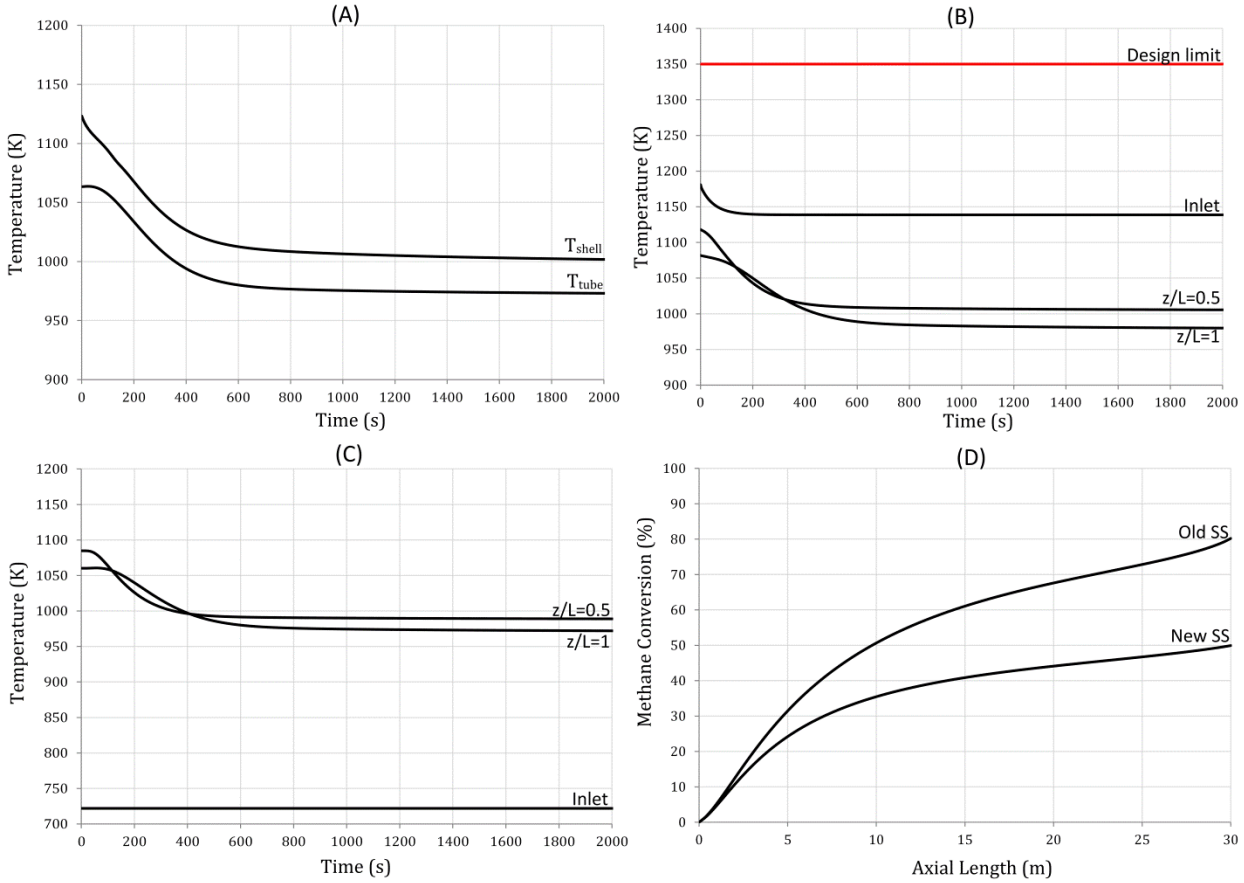

Figure 14: Effect of step decrease in coal-derived syngas feed by 50% for co-current configuration on (a) exit gas temperature leaving the tube and shell, (b) tube wall temperature at the inlet, exit, and halfway point, (c) catalyst core temperature at the inlet, exit, and halfway point and (d) axial methane conversion.

For the counter-current configuration, the system response to a similar change is shown in Figure 15. The shell gas temperature decreases by 125 K to 850 K while the exit tube gas temperature drops to

1060 K. Figure 15B shows that the maximum tube wall temperature at the tube exit moves further away from the design limit temperature and reaches 1240 K. Though the magnitude of change is different from the co-current mode, the trends are similar with the catalyst core and tube wall temperatures decreasing. Also, the methane conversion drops as expected but the change is higher at 33% points. Both sets of simulations demonstrate that in the event the gasifier is to be turned down for load following purposes or in the event of a failure of one of the coal hoppers where the feed drops significantly, the integrated system can operate safely.

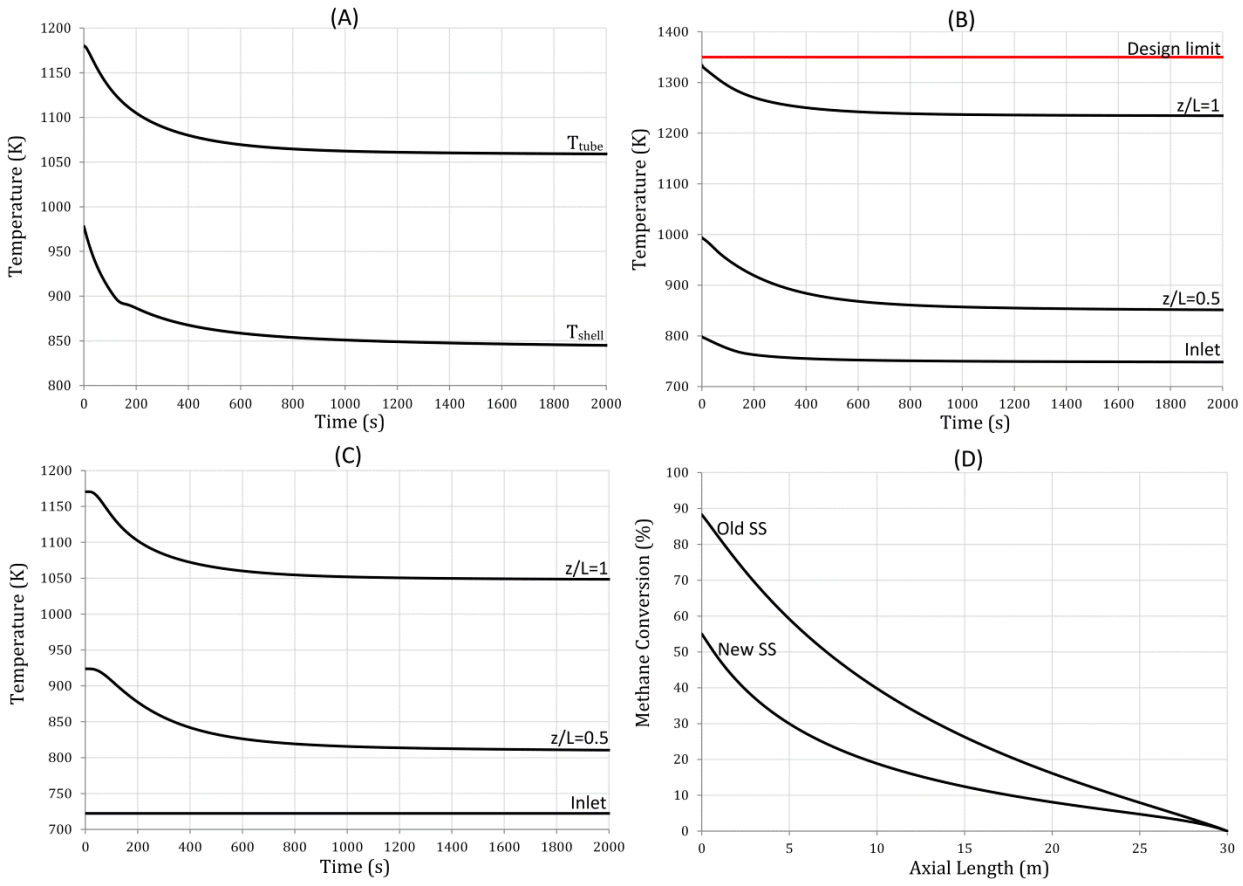

Figure 15: Effect of step decrease in coal-derived syngas feed by 50% for counter-current configuration on (a) exit gas temperature leaving the tube and shell, (b) tube wall temperature at the inlet, exit, and halfway point, (c) catalyst core temperature at the inlet, exit, and halfway point and (d) axial methane conversion.

5. Open loop start-up procedure

The simulations for the transient modes of operation in the previous sections demonstrated that the co-current configuration is safer to operate in transient modes than the counter-current configuration for flexible polygeneration. However, the transient modes are initiated from an operating steady-state that was established in our previous study. Though the designs show flexible operation, the question remains if the integrated system can reach the operating steady-state from a cold start condition. Furthermore, the start-up procedures for the gasifier and steam methane reformer are complex even when operated independently and hence, the start-up procedure for the integrated system needs to be investigated. In the current study the start-up procedure for the integrated system has been adopted from existing industrial practices that are used for gasifier and steam reformer start-ups. This methodology helps to establish a realistic start-up procedure for the integrated system.

Typically, for an entrained-bed gasifier, the start-up is done by slowly increasing the refractory temperature over a period of two days. Natural gas burners are employed to increase the system temperature and coal feed is introduced once the gasifier operating temperatures are reached. The critical constraint during the start-up is the maximum allowed heating rate of the refractory layer of the gasifer which is usually limited to 10-20°C/min [13]. Monaghan and Ghoniem [12] simulated the start-up of a GE entrained bed gasifier using dynamic models that were implemented in Aspen custom modeller such that the heating rate is less than 10°C/min for the refractory. However, in all of the afore-mentioned references there were no details about the operation of the radiant syngas cooler during the start-up. It is assumed that the radiant cooler is brought online at some point during the start-up until which the quench cooler is employed to cool the natural gas combustion gases.

Contrary to the gasifier start-up, the steam reformer start-up is relatively fast but it involves a series of steps to ensure that the reformer tubes are not damaged. The first step in the reformer start-up usually involves nitrogen circulation through the reformer tubes [14], [15]. Simultaneously, the furnace burners are ignited and the system temperature is slowly increased such that no hot spots are formed on the tube walls. Steam is then introduced into the tubes but is only done when the reformer tube exit temperature is higher than that of the dew point of the steam being introduced. This is important to ensure that steam does not condense on the catalyst which may later expand when heat duty to the reformer is increased resulting in an explosion and damaging the tubes [16]. After steam injection, the reformer is allowed to reach the operating temperatures at which point natural gas is slowly introduced. During this phase, a high H_2O/C ratio is maintained. The natural gas feed is then slowly increased to the rated capacity and the steam injection is altered to meet the desired H_2O/C ratio at the inlet.

For the integrated system, the start-up procedure has been established based on the procedures that are currently implemented for the individual systems. However, for the integrated system there are some limitations: First, unlike in a conventional reformer where the furnace temperature can be controlled, the shell side temperature cannot be controlled during the start-up which may affect the reformer operation. Second, the start-up time scales for the reformer and the gasifier are different which means that the reformer comes online before the gasifier. In this study, the gasifier was not modelled but the gasifier exit temperature serves as inlet conditions for the radiant cooler. The gasifier exit temperature was simulated using regressed models as a function of time based on the simulation data from Monaghan and Ghoniem [12], [17] for a GE entrained-bed gasifier. The gasifier exit temperature increase rapidly for the first hour when natural gas and air is combusted in the burner, after which the temperature gradually increases until coal feed is introduced. For the reformer, the following sequences of steps are followed:

(i) Nitrogen is introduced to the reformer tubes and continued until the tube gas exit temperature is greater than 575 K.

(ii) Nitrogen flow to the tubes is decreased and steam at 550 K is introduced. This was continued until the tube gas exit temperature reached 750 K.

(iii) Natural gas at 50% of the steady-state capacity (530 kmol/h) is then introduced. The steam flow through the tubes is maintained such that the H_2O/C ratio at the inlet is equal to 5.

(iv) The H_2O/C is reduced to the operating range of 3.3 after one hour. The natural gas supply is maintained at 50% until the gasifier operating temperature is reached.

(v) Once the gasifier is online, the natural gas supply to the reformer tubes is increased to 80% of the steady-state operating capacity as the heat load to the reformer tubes increases.

(vi) The reformer is then slowly brought to 100% capacity with a series of step changes in natural gas flow rates that is made in one hour intervals.

Figure 16 shows the shell and reformer gas temperature profiles during the start-up. The reduced order model for the RSC inlet temperature ensures that the trajectory is similar to that occurring during a gasifier start-up. It can be seen that the tube gas exit temperature increase rapidly in the first two hours that allows for the natural gas feed to be introduced within three hours from start-up. The high H_2O/C ratio when natural gas is introduced initially increases the rate of the exothermic water gas shift reaction and thereby increases the reformer gas temperature for a brief period of time. Figure 17 shows the effect of the increased rate of water gas shift reaction on the tube gas mole fraction profiles during this period. The amount of CO_2 at the exit increases rapidly when high H_2O/C ratio is maintained and starts to decrease when the ratio is reset to 3. As the temperature continues to increase gradually, the rate of endothermic reforming reaction increases. The gasifier operating temperature is reached around 21 hours into the start-up at which point natural gas combustion is stopped and coal water slurry is introduced into the gasifier. This change is introduced as a step change in the simulation even though

the process takes 2-3 hours during the actual start-up. However, the step change is sufficient to detect any violations in operating constraints. At this stage, the natural gas feed to the reformer tubes is increased to 80% of the capacity at steady-state. The natural gas feed is then gradually increased every hour to the operating capacity of 1061 kmol/hr and the reformer exit temperature continues to drop as the methane conversion increases. The integrated system takes approximately 40 hours to reach operational steady-state from a cold start condition.

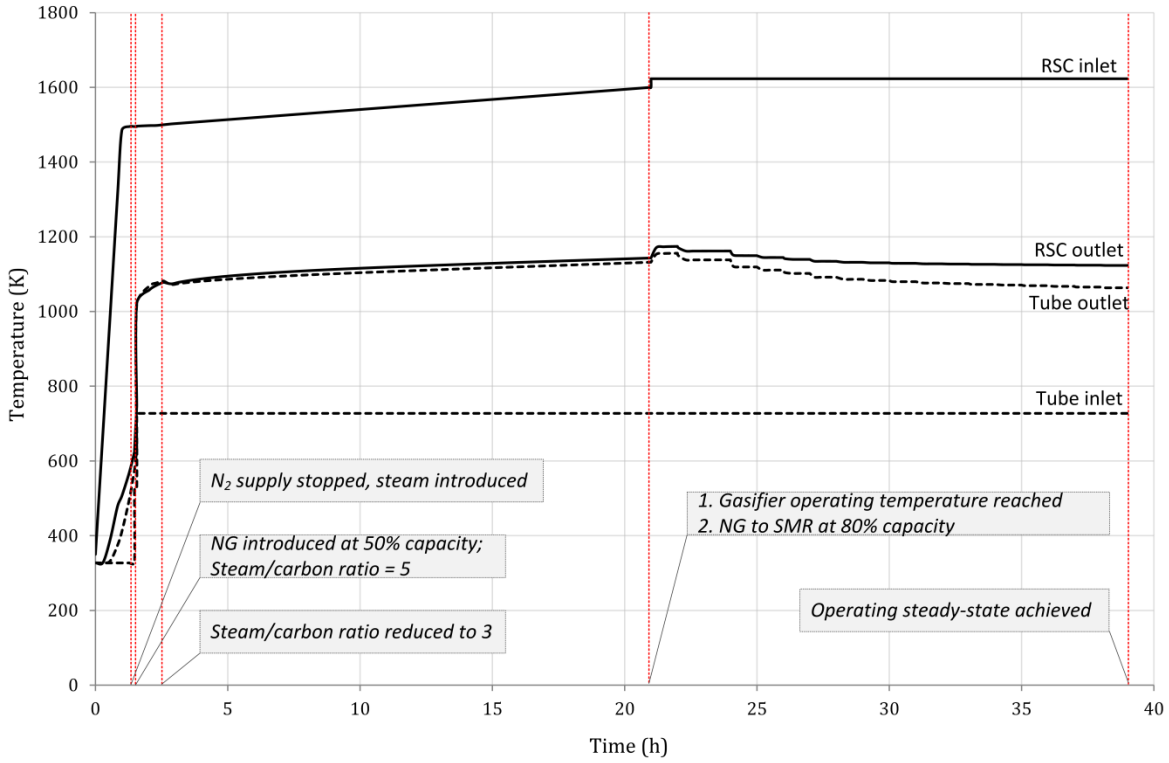

Figure 16: Shell gas and reformer tube gas temperature profiles during start-up

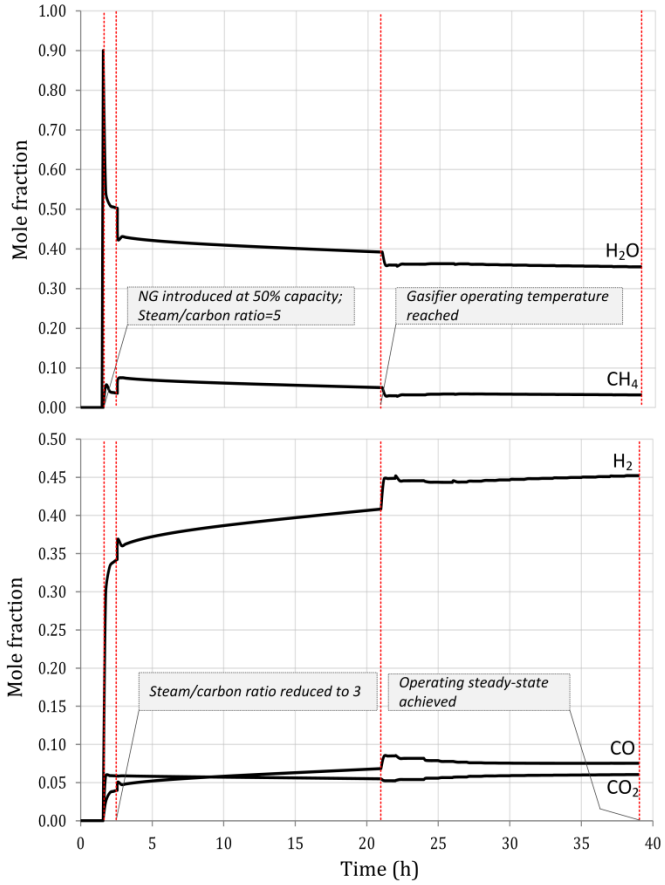

Figure 17: Tube gas mole fraction profiles at reformer exit during start-up

Figure 18 shows the catalyst core temperature profiles during start-up at different locations along the length of reformer tubes. The profiles shows hot spots at t=21 hours when the gasifier comes online and when the natural gas feed to the reformer is increased. It can also be observed that the location of the hot spot along the axial direction changes during the course of the start-up. During the first 20 hours of the start-up, the hottest region is nearer to the exit of the reformer. However, the increase in natural gas flow rates when the gasifier comes online results in a higher pressure drop in the reformer tubes. This low pressure near the exit of the reformer further favors the reforming reaction which decreases temperature of the catalyst core near the reformer outlet. Though hots spots are observed during start-up, the temperature gradient is low and shows that the start-up can be done without any damage to the catalyst bed. Another key operational constraint is the maximum tube wall temperature. Figure 19 shows the maximum tube wall temperature during the start-up phase. The maximum temperature

does not exceed the design limit temperature of 1350 K for the integrated system. During the start-up phase, the maximum temperature reaches 1214 K when the gasifier comes online but later decreases to a steady-state value of 1180 K.

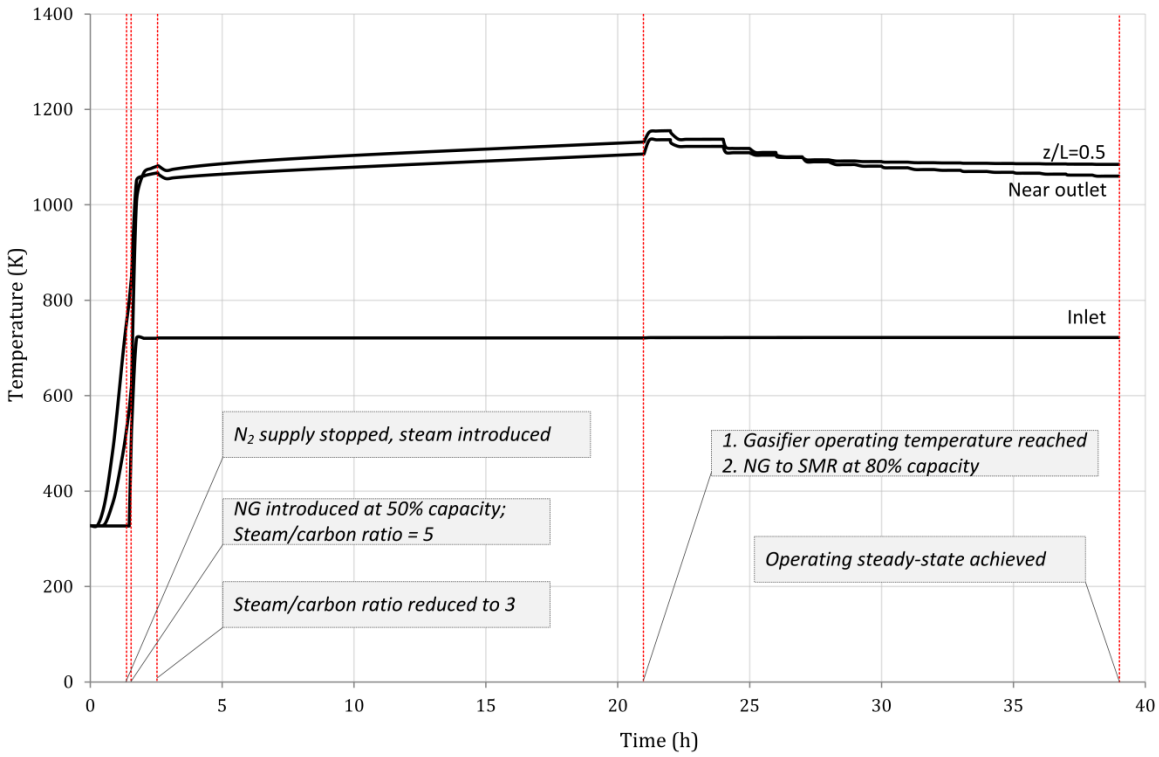

Figure 18: Catalyst core temperature profiles along the reformer tubes during start-up

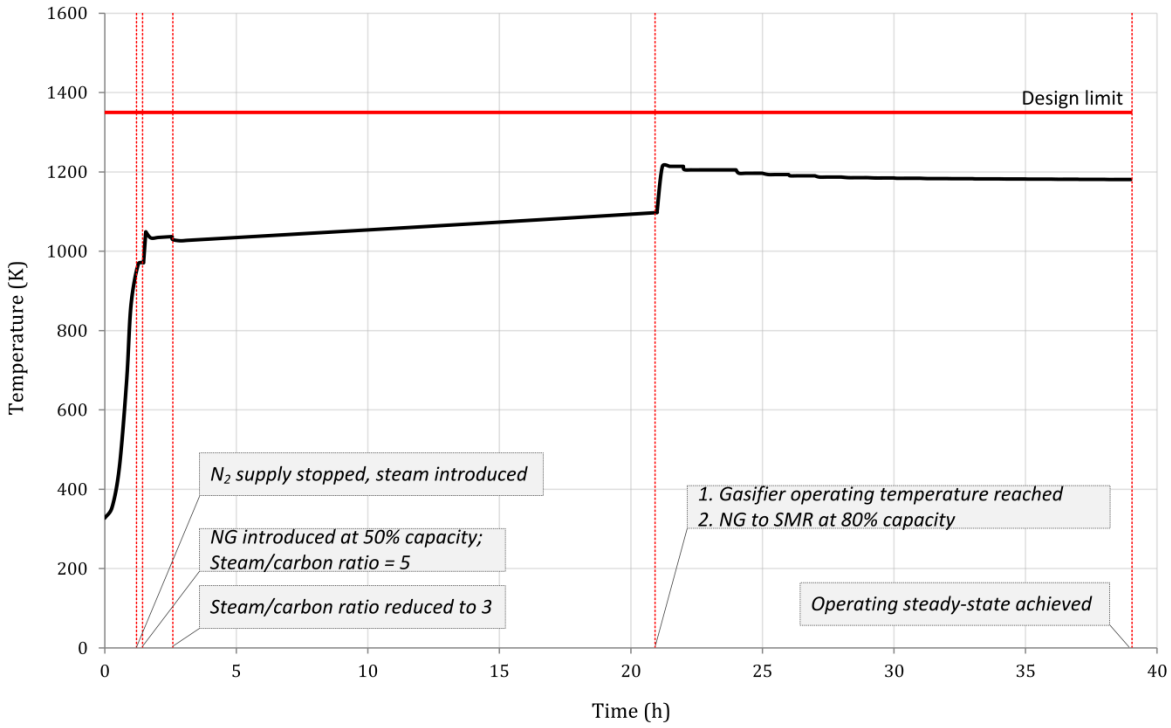

Figure 19: Maximum tube wall temperature profile during start-up

6. Conclusions

The first-principles based model that was previously developed for the integrated RSC and SMR was utilized in this work to study the dynamic operability. The system was subjected to step changes in manipulated variables on the reformer side to assess the impact on the integrated system performance. For example, it was observed that the inlet H_2O/C ratio could be an important manipulated variable to control the product H_2/CO molar ratio. The system was also subjected to reduced natural gas and steam feeds (a 25% decrease from the nominal operating point) to the SMR tubes to determine the dynamic flexibility of the integrated system. The open-loop simulations helped build an understanding of the integrated system dynamics and also helped identify variables that were more likely to violate the operating constraints.

Though the feasibility of the integrated RSC/SMR concept at steady-state was previously demonstrated, it did not shed light in terms of operational safety and flexibility. The results presented in this work show that the co-current configuration, though having reduced methane conversion of 80% compared to the 88% methane conversion in counter-current configuration and smaller processing capacity by design, is more flexible than the counter-current configuration for operations in a transient mode where the shift to a new operating point is feasible. Also, the start-up procedure established for the co-current configuration showed the possibility of safely starting up the integrated system where the natural gas reformer comes online within a few hours from a cold start condition. One of the major drawbacks observed for the counter-current configuration was the limited margin available to withstand disturbances because of the proximity of the maximum tube wall temperature at 1334 K near the RSC inlet to the design limit of 1350 K. At present, it can be concluded that the co-current configuration is the safer and more flexible design option for the proposed integrated system. This design conclusion for the integrated system is consistent with the design philosophy for conventional top-fired steam reformers. In conventional reformers, the feed to the tubes is introduced at the top where the tube wall temperatures are high, ensuring that rate of cooling are highest at the hottest parts of the reformer. However, it is possible that a new design variant of the counter-current configuration could be used which provides additional cooling to the top of the wall through some other means. This would increase the safety margin for the tube wall temperatures while also maintaining the benefits of higher methane conversions. Alternatively, it may be possible to design a control system which is able to reject the disturbances safely for counter-current mode, which is the subject of future work.

ACKNOWLEDGEMENTS:

Financial support from Imperial Oil University Research Award, NSERC Discovery Grant and NSERC – Collaborative Research and Development grant are gratefully acknowledged.

REFERENCE:

[1] "Tampa Electric Polk Power Station Integrated Gasification Combined Cycle Project - Final Technical Report," U.S. DOE and Tampa Electric Company, 2002.

[2] T. A. Adams II and P. I. Barton, "Combining coal gasification and natural gas reforming for efficient polygeneration," *Fuel Process. Technol.*, vol. 92, no. 3, pp. 639–655, Mar. 2011.

[3] J. H. Ghouse, D. Seepersad, and T. A. Adams, "Modelling, simulation and design of an integrated radiant syngas cooler and steam methane reformer for use with coal gasification," *Fuel Process. Technol.*, vol. 138, pp. 378–389, 2015.

[4] Y. Chen, T. A. Adams II, and P. I. Barton, "Optimal Design and Operation of Flexible Energy Polygeneration Systems," *Ind. Eng. Chem. Res.*, vol. 50, pp. 4553–4566, 2011.

[5] W. Cho, T. Song, A. Mitsos, J. T. Mckinnon, G. H. Ko, J. E. Tolsma, D. Denholm, and T. Park, "Optimal design and operation of a natural gas tri-reforming reactor for DME synthesis," *Catal. Today*, vol. 139, pp. 261–267, 2009.

[6] Y. K. Salkuyeh and T. A. Adams, "Combining coal gasification, natural gas reforming, and external carbonless heat for efficient production of gasoline and diesel with CO2 capture and sequestration," *Energy Convers. Manag.*, vol. 74, pp. 492–504, 2013.

[7] C. Higman and S. Tam, "Advances in Coal Gasification, Hydrogenation, and Gas Treating for the Production of Chemicals and Fuels," *Chem. Rev.*, vol. 114, no. 3, pp. 1673–1708, Oct. 2013.

[8] "gPROMS." Process Systems Enterprise.

[9] C. J. Lim and J. R. Grace, "On the Reported Attempts to Radically Improve the Performance of the Steam Methane Reforming Reactor," *Can. J. Chem. Eng.*, vol. 74, 1996.

[10] J. Xu, C. M. Y. Yeung, J. Ni, F. Meunier, N. Acerbi, M. Fowles, and S. C. Tsang, "Methane steam

reforming for hydrogen production using low water-ratios without carbon formation over ceria coated Ni catalysts," *Appl. Catal. A Gen.*, vol. 345, no. 2, pp. 119–127, Aug. 2008.

[11] P. J. Robinson and W. L. Luyben, "Simple Dynamic Gasifier Model That Runs in Aspen Dynamics," *Ind. Eng. Chem. Res.*, vol. 47, no. 20, pp. 7784–7792, Oct. 2008.

[12] R. F. D. Monaghan and A. F. Ghoniem, "Simulation of a Commercial-Scale Entrained Flow Gasifier Using a Dynamic Reduced Order Model," *Energy & Fuels*, vol. 26, no. 2, pp. 1089–1106, Feb. 2012.

[13] K. V.S. and B. I.P., "Determing the maximum possible rates of single sided heating of refractories," *Ogneupory*, no. 4, pp. 51–55, 1971.

[14] Asia Industrial Gases Association, "Safe Startup and Shutdown Practices for Steam Reformers." 2013.

[15] European Industrial Gases Association AISBL, "Combustion Safety for Steam Reformer Operation."

[16] M. Rogers, "Lessons Learned From an Unusual Hydrogen Reformer Furnace Failure," Fort McMurray, Alberta, 2005.

[17] R. F. D. Monaghan, "Dynamic Reduced Order Modeling of Entrained Flow Gasifiers by," MIT, 2010.